Multi-Sensor Terrain Classification for Safe Spacecraft Landing

AYANNA HOWARD, Senior Member, IEEE
HOMAYOUN SERAJI, Fellow, IEEE
Jet Propulsion Laboratory

A novel multi-sensor information fusion methodology for intelligent terrain classification is presented. The focus of this research is to analyze safety characteristics of the terrain using imagery data obtained by on-board sensors during spacecraft descent. This information can be used to enable the spacecraft to land safely on a planetary surface. The focus of our approach is on robust terrain analysis and information fusion in which the terrain is analyzed using multiple sensors and the extracted terrain characteristics are combined to select safe landing sites for touchdown. The novelty of this method is the incorporation of the T-Hazard Map, a multi-valued map representing the risk associated with landing on a planetary surface. The fusion method is explained in detail in this paper and computer simulation results are presented to validate the approach.

Manuscript received October 10, 2001; revised June 3, 2004; released for publication July 22, 2004.

IEEE Log No. T-AES/40/4/836508.

Refereeing of this contribution was handled by M. Ruggieri.

This work was performed at the Jet Propulsion Laboratory, California Institute of Technology, under contract with the National Aeronautics and Space Administration.

Authors' address: Jet Propulsion Laboratory, California Institute of Technology, 4800 Oak Grove Drive, M/S 198-219, Pasadena, CA 91109-8099.

0018-9251/04/$17.00 © 2004 IEEE

I. INTRODUCTION AND BACKGROUND

The safety of the landing site is without question the single most important factor in NASA landed exploration missions, for the simple reason that there will be no science return if the spacecraft does not land safely [1–3]. The current practice for selecting safe landing sites is based on human visual examination of prior aerial images of potential landing sites obtained from orbital imagery. In the Mars exploration rover (MER) mission, the landing site selection process was driven by science return and safety constraints. The Mars surface data was extracted from Mars orbiter camera (MOC) and thermal emission imaging system (THEMIS) images obtained by the Mars global surveyor (MGS) and Mars Odyssey missions. In all NASA landed missions thus far, once the landing site is selected, the spacecraft performs a blind landing operation with no provision for corrective maneuvers prior to touchdown. This approach would be satisfactory if precise landing accuracy of the spacecraft and accurate prior knowledge of the landing site characteristics could be achieved. However, these requirements are not met in practice, and consequently the mission designers have to select a large, safe, but scientifically less interesting site for spacecraft landing.

Typically, engineering criteria established for ensuring success of the mission are constructed by analyzing terrain characteristics that affect the ability of the spacecraft to land safely on a planetary surface. The roughness of the terrain and the size/concentration of rocks must be minimal. The surface slope must be within acceptable limits since the spacecraft may become unstable at certain angles. In most cases, the following are the major hazards affecting the landing site choices [1]:

smoothness: relatively few craters and boulders,
approach: no large hills, high cliffs, or deep craters,
slope: minimum slope at the point of touchdown.

Prior research on hazard assessment has focused mainly on a single terrain sensor, such as a lidar or a camera. A lidar model (incorporating parameters such as beam divergence and detector noise) as well as an algorithm to determine slope and roughness (by local plane fitting and outlier detection) has been developed and tested on a rocket sled approaching a synthetic terrain [4–5]. Visible image algorithms have also been developed to determine slope and roughness from multiple images (using feature tracking and homography estimation to determine the best fit plane and residual error) [6], as well as hazard (rock and crater) detection based on image segmentation and shadow detection [7]. Other approaches have combined hazard maps and confidence maps, along with previously selected sites, the distance to the original site, and a fuel-based reachability score

to determine the best site [8]. Overall, the current state-of-the-art (SOA) in hazard assessment uses a single terrain sensor that is susceptible to failure and may produce noisy information due to environmental conditions such as spacecraft jitter. In addition, conventional methods for classification of terrain hazards use a binary representation, i.e., the terrain is designated as either safe or unsafe. To provide tolerance to single-sensor failure, as well as to utilize diverse sources of data for hazard assessment in a robust manner, our research focuses on the use of multiple active and passive terrain sensors that classify the terrain based on a gradual representation of terrain safety. This process provides a much finer resolution in terrain classification, and consequently a more efficient process for safe site selection. By focusing on the process of intelligent information fusion of data retrieved from multiple heterogeneous sensors, the sensory data can be used to analyze the approaching terrain for hazards and continuously select sites deemed safe for spacecraft landing. This enables any trajectory adjustments to occur in the thruster command sequence in order to reduce mission costs and risk by ensuring spacecraft survivability during the landing process.

II. TECHNIQUE

We discuss the process of multi-sensor information fusion, rather than multi-sensor data fusion. Data fusion is the process of integrating actual data measurements extracted from different sensors and combining them into one representation. Information fusion is the process of using information derived from multiple sensors and combining them at the information level. There are various research efforts focused on multi-sensor data fusion [9], with a primary focus on statistical methods (Kalman filters) and probabilistic techniques (Bayesian network). Probabilistic techniques focus on combining data from multiple sensors by using weighting factors based on how accurate the sensor data is, whereas statistical methods concentrate on minimizing errors between actual values and predicted values. The framework we employ for multi-sensor information fusion is to combine hazard information derived from different sensors into a global scene description. For our application, we utilize three terrain sensors: lidar, radar, and camera. The terrain information extracted from the lidar and radar sensors include roughness and slope information. As the camera sensor employs a monocular vision system, the information detectable by the camera sensor include roughness derived from topographic features. We show later how the difference in the type of information extracted from the diverse sensor suite extends the capability of the hazard assessment system to recognize hazards that a single sensor is unable to detect.

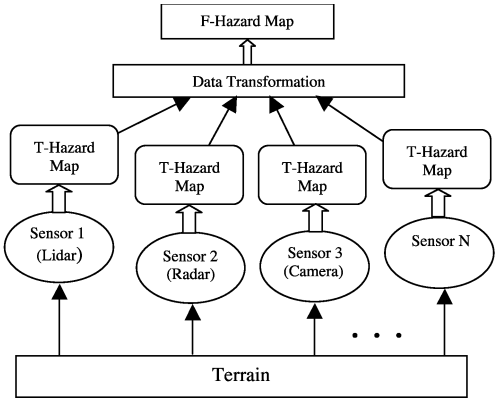

Fig. 1. Overview of multi-sensor information fusion approach.

To quantify potential hazard information, terrain characteristics are extracted from each sensor's data set and the risk associated with landing on a surface with the given characteristics is represented using the terrain hazard map (T-hazard map). In order to effectively combine this heterogeneous data set, the hazard maps are aligned using a combination of rotation, translation, and scaling. This process, called data transformation, allows us to compensate for sensor parameter differences such as different fields-of-view, resolutions, and pointing locations, and allows the formation of a unified hazard map that represents a global view of the terrain. Once transformed, individual hazard maps are combined into a fused hazard map (F-hazard map) representation of the terrain. The overview of this approach is depicted in Fig. 1.

A. Terrain Hazard Map Construction

To enable safe landing of a spacecraft on a planetary body, we utilize a lidar, radar, and camera sensor for multi-sensor information fusion. The methodology presented here, however, is applicable to n (> 3) heterogeneous sensors. Each sensor images the terrain and associated data values are used to compute a T-hazard map, which represents the risk of the terrain for spacecraft landing using a fuzzy-logic construct. The T-hazard map is represented by a grid of cells in which each cell is associated with a region physically located on the terrain surface.

Fuzzy logic [10] provides a linguistic-based method for modeling the relationship between data input values (such as range data) and hazard information. Fuzzy logic can inherently handle the uncertainties in the sensor data input and allow mission designers to describe, in plain English, how to quantify terrain safety without having to describe the complex behavior of the selection process itself. The application of fuzzy logic to solve the landing site classification problem is motivated by its ability to incorporate the mission designer's

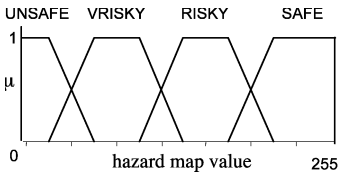

Fig. 2. Membership functions representing T-hazard map values.

expert knowledge directly into the system, its noise tolerance to the imagery data retrieved from sensors, and its ability for real-time implementation while ensuring robustness with respect to imprecise or uncertain image interpretation. In fact, fuzzy logic is ideally suited for this application because it naturally copes with ambiguities and imprecisions that exist in terrain images due to motions and vibrations of the spacecraft. This is accomplished by representing terrain information using ranges of values that are sectored into several linguistic classes that have smooth overlapping boundaries.

The entry-descent-landing (EDL) operations of a spacecraft occur over a very short period of time, typically on the order of 1–5 min. Therefore, the computational speed of any algorithm used for terrain analysis is of utmost importance. The terrain sensors are mounted on the spacecraft, which is moving rapidly toward the surface. Vibrations and jitters induced in the terrain sensors generate imprecision in the sensory data in the form of noise. Furthermore, there are inherent uncertainties associated with interpreting the sensed data (e.g. shadows in the camera image can be misinterpreted as rocks on the landing site). Therefore, uncertainty management is an important factor for any robust terrain assessment method. Fuzzy logic rule evaluation involves only simple arithmetic calculations that can be performed very rapidly. Therefore, the computational time of creating the T-hazard map using fuzzy logic is very small, making it feasible for real-time implementation. By utilizing the fuzzy logic framework, the T-hazard map can efficiently represent the level of risk (or safety) involved with landing on a specific site. For our purposes, the T-hazard map is represented by the linguistic fuzzy sets {SAFE, RISKY, VERY-RISKY, UNSAFE} and their membership functions are shown in Fig. 2 using the gray-scale (0–255) representation.

B. Lidar and Radar Terrain Hazard Map Construction

The data extracted from both active sensors, lidar, and radar, reflects the elevation or height of surface features embedded within the viewable terrain region. Both sensors provide range data that is converted into an elevation map for extraction of terrain characteristics such as terrain slope and roughness. The main difference in the data values returned by the lidar and radar sensors is caused by the differences between field-of-view, range of operation, and resolution parameters. The derived elevation data is used to extract slope and roughness characteristics of the terrain using a least-squares plane fitting algorithm [4–5]. The slope of the plane which best fits the elevation points is used as the terrain slope value, and the roughness is then computed as the residual of the fit. Once calculated, the slope and roughness values are fed into a fuzzy-logic rule base [11] to compute values for the T-hazard map. The fuzzy logic rules are used to classify the risk of the terrain for spacecraft landing based on the terrain characteristics present in the given data set. In order to construct the hazard map, the terrain characteristics are first converted into a linguistic representation using fuzzy logic sets. The roughness is represented by the linguistic fuzzy sets {SMOOTH, ROUGH, ROCKY}, while the terrain slope parameter is converted into the linguistic representations {FLAT, SLOPED, STEEP}. The membership functions of these sets are then input into a set of fuzzy logic rules used to classify the terrain (Table I). The output from the rule-base represents the relative level of safety associated with the viewable area.

TABLE I
Fuzzy Rule Base for Constructing Terrain Hazard Map

Slope	Roughness	T-hazard Map Value
FLAT	SMOOTH	SAFE
FLAT	ROUGH	RISKY
SLOPED	SMOOTH	RISKY
SLOPED	ROUGH	VRISKY
STEEP		UNSAFE
	ROCKY	UNSAFE

Note: Empty fields in fuzzy rule base indicate specified input parameter has no effect on rule outcome.

As an example, the rules associated with the first and last rows in the table are as follows.

If slope is flat and roughness is smooth, then terrain is safe.
If roughness is rocky, then terrain is unsafe.

C. Camera Terrain Hazard Map Construction

For construction of the hazard map based on camera imagery data, we utilize a variation on a simple intensity-based algorithm [6] that determines roughness based on pixel standard deviation for a given region using the following equations:

$$I_m = \frac{\sum_{i,j\in w} I_{i,j}}{N * M}, \qquad V = \sqrt{\frac{\sum_{i,j\in w}(I_m - I_{i,j})^2}{N * M}} \quad (1)$$

where V is the standard deviation, I is pixel intensity, I_m is average pixel intensity within the window, w is a window surrounding, $N * M$ is the size of window w, and i, j is the location of the pixel in

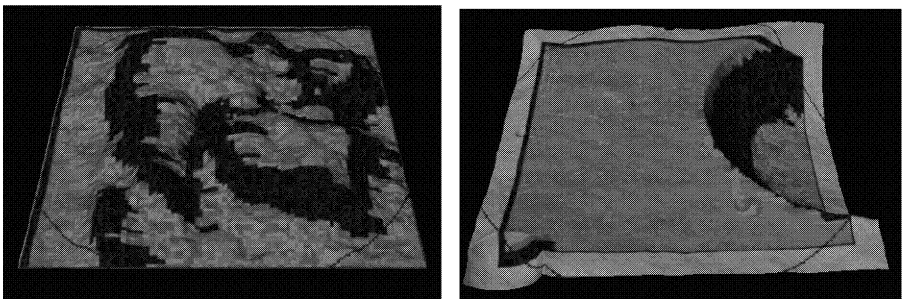

Fig. 3. Computed hazard maps overlaid on terrain imagery data.

the image. Equation (1) associates large surface variations with rougher surface areas. These roughness values are subsequently used to construct the T-hazard map by feeding in the value of V into a fuzzy-logic rule-base. The camera roughness characteristic is represented by the linguistic fuzzy sets {SMOOTH, ROUGH, VERY-ROUGH, ROCKY}. In addition, although we currently utilize a monocular camera system, the inclusion of stereo images or using two consecutive mono images allows additional characteristics, such as slope, to be incorporated into computing the risk associated with landing using the rule-set depicted in Table I. For our purposes, the following rule-set is used to compute the landing risk.

If roughness is smooth, then terrain is safe.
If roughness is rough, then terrain is risky.
If roughness is very-rough, then terrain is very-risky.
If roughness is rocky, then terrain is unsafe.

Fig. 3 shows example images of computing the T-hazard map based on visual imagery using this fuzzy-logic construct. In this figure, safe cells are represented by light gray, unsafe cells by black, and gray-level cells represent hazards with risky and very risky values.

D. Data Transformation

Once the individual hazard maps are computed, we must correctly align the maps so that they reference the same global areas of the terrain surface. This is accomplished by using a data transformation process that accounts for differences in each sensor's operating parameters.

The first step in the data transformation process (Fig. 4) is to find the centroid offset of each sensor's hazard map based on the sensor's pointing direction. Given the mounting position and orientation of the sensor relative to the spacecraft reference origin, and the current distance of the spacecraft with respect to the terrain surface, the following equation is used to determine the viewable area of the terrain which the sensor is able to image:

$$o_y = h\tan\theta_y + o'_y \tag{2}$$

$$o_x = h\tan\theta_x + o'_x \tag{3}$$

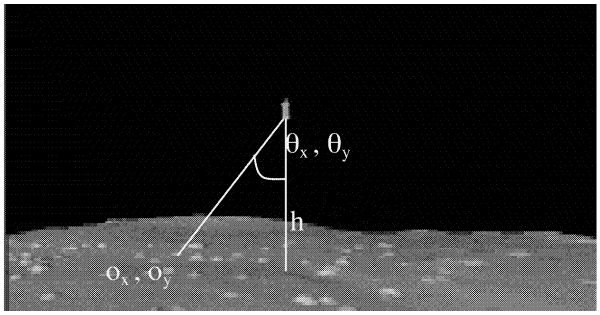

Fig. 4. Determining sensor offset in data transformation process.

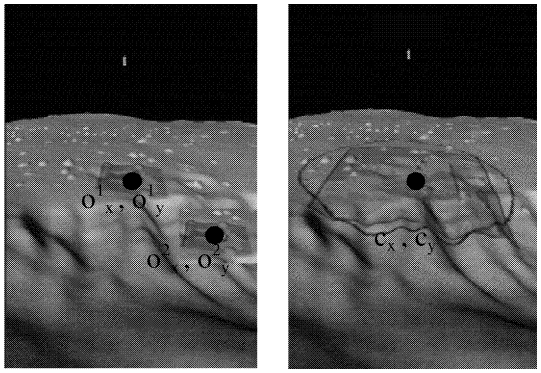

Fig. 5. Determining translation parameters in data transformation process.

where (θ_x,θ_y) are the angle offsets of the sensor from the spacecraft normal, h is the distance of the spacecraft from the planet surface, (o'_x,o'_y) are the position offsets of the sensor from the spacecraft reference origin, and (o_x,o_y) are the new centroid offsets for each sensor. Once calculated, the sensor offset is used to translate each sensor hazard map into the same reference coordinate system (Fig. 5). A new center (c_x,c_y) of the fused hazard map is calculated by averaging the distance between the sensors' centroid offsets. The new center is used in order to determine the amount of individual translation required for each hazard map using the following equation:

$$(c_x,c_y) = \left(\frac{\sum_{i=1}^{n} \frac{o_x^i}{r^i}}{n}, \frac{\sum_{i=1}^{n} \frac{o_y^i}{r^i}}{n} \right) \tag{4}$$

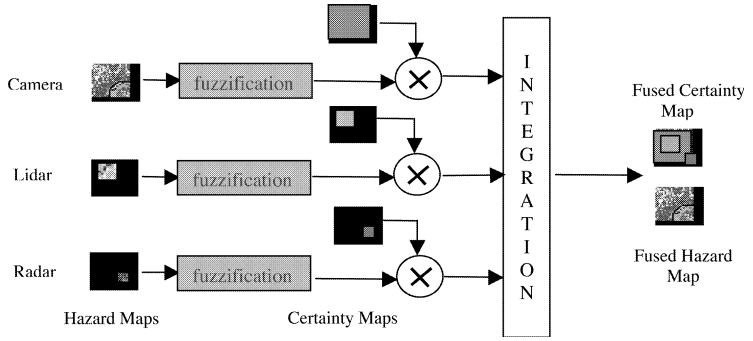

Fig. 6. F-hazard map construction.

where r represents the map resolution, and n is the number of on-board spacecraft sensors.

Because different sensors have different fields-of-view, their imaging areas of the terrain are not the same. After the new center is calculated, the actual hazard map centroid location is translated by adding border grid cells that enlarge the image so that all imaging areas match to the largest one. For this case, border cells are given values of unknown since hazard values are not actually calculated for these added cells. Once translated, each hazard map is then scaled to equivalent resolution and size constraints. This is accomplished by enlarging each hazard map to account for the lowest resolution and the maximum image size. Due to differences in resolution, size, and sensor offsets, data may not be available from the original hazard map to populate the newly enlarged hazard map. In this case, newly added cells are given the value of unknown.

Once all hazard maps are transformed into the same reference plane, they are fused together to provide a global representation of the terrain.

E. Terrain Hazard Map Fusion

Each T-hazard map is constructed independently of one another and generates values based on sensed data obtained from one on-board terrain sensor. In addition, associated with each terrain sensor is a variable confidence factor that represents the certainty in the sensory data. This factor is generated automatically by a set of user-specified rule statements that are based on the sensor characteristics and environmental conditions. Hazard map information is thus combined by utilizing numeric certainty factors to create an F-hazard map representation of the terrain (Fig. 6). We use the concept of "behavior integration" in behavior-based control architectures in which recommendations from different behaviors are integrated to form a unified control action [12, 13]. In this same way, we blend together individual hazard maps to ensure that each sensor is allowed to influence the final terrain representation. The F-hazard

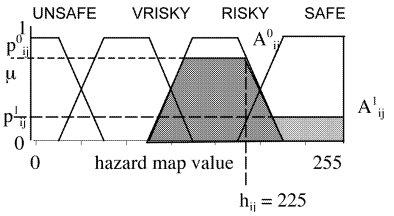

Fig. 7. Fuzzifying hazard map values.

map is computed using the following equation:

$$H_{i,j} = \frac{\sum_{k=1}^{n} \left(\beta_{i,j}^{k} \sum p_{i,j}^{k} A_{i,j}^{k} \right)}{\sum_{k=1}^{n} \left(\beta_{i,j}^{k} \sum A_{i,j}^{k} \right)} \tag{5}$$

where i, j is the index of each cell in the T-hazard map, $H_{i,j}$ is the fused T-hazard map value computed for each cell, n is the number of on-board terrain sensors, $\beta_{i,j}$ represents the certainty factor associated with each cell, $p_{i,j}$ is the peak value associated with fuzzifying the hazard map values ($h_{i,j}$) for each sensor, and $A_{i,j}$ is the area under the hazard membership function associated with the hazard value (Fig. 7).

Given that we currently utilize three sensors, camera, lidar, and radar, (5) becomes

$$H_{i,j} = \frac{\beta_{i,j}^{\mathrm{C}} \sum p_{i,j}^{\mathrm{C}} A_{i,j}^{\mathrm{C}} + \beta_{i,j}^{\mathrm{R}} \sum p_{i,j}^{\mathrm{R}} A_{i,j}^{\mathrm{R}} + \beta_{i,j}^{\mathrm{L}} \sum p_{i,j}^{\mathrm{L}} A_{i,j}^{\mathrm{L}}}{\beta_{i,j}^{\mathrm{C}} \sum A_{i,j}^{\mathrm{C}} + \beta_{i,j}^{\mathrm{R}} \sum A_{i,j}^{\mathrm{R}} + \beta_{i,j}^{\mathrm{L}} \sum A_{i,j}^{\mathrm{L}}} \tag{6}$$

where C, L, and R represent the camera, lidar, and radar sensors, respectively, and the certainty factors β^{C}, β^{L}, and β^{R} represent the strengths by which the individual hazard map values influence the final construction of the fused hazard map.

The certainty factors are computed by three sets of certainty rules, where distance denotes the physical distance of the spacecraft to the surface and is represented by the linguistic fuzzy sets {NEAR, DISTANT, FAR}. The certainty factors are represented by the linguistic fuzzy sets {LOW, MEDIUM, HIGH}, and are constructed based on the sensor operating parameters as depicted in Table II and Fig. 8. From Fig. 8 we note that the

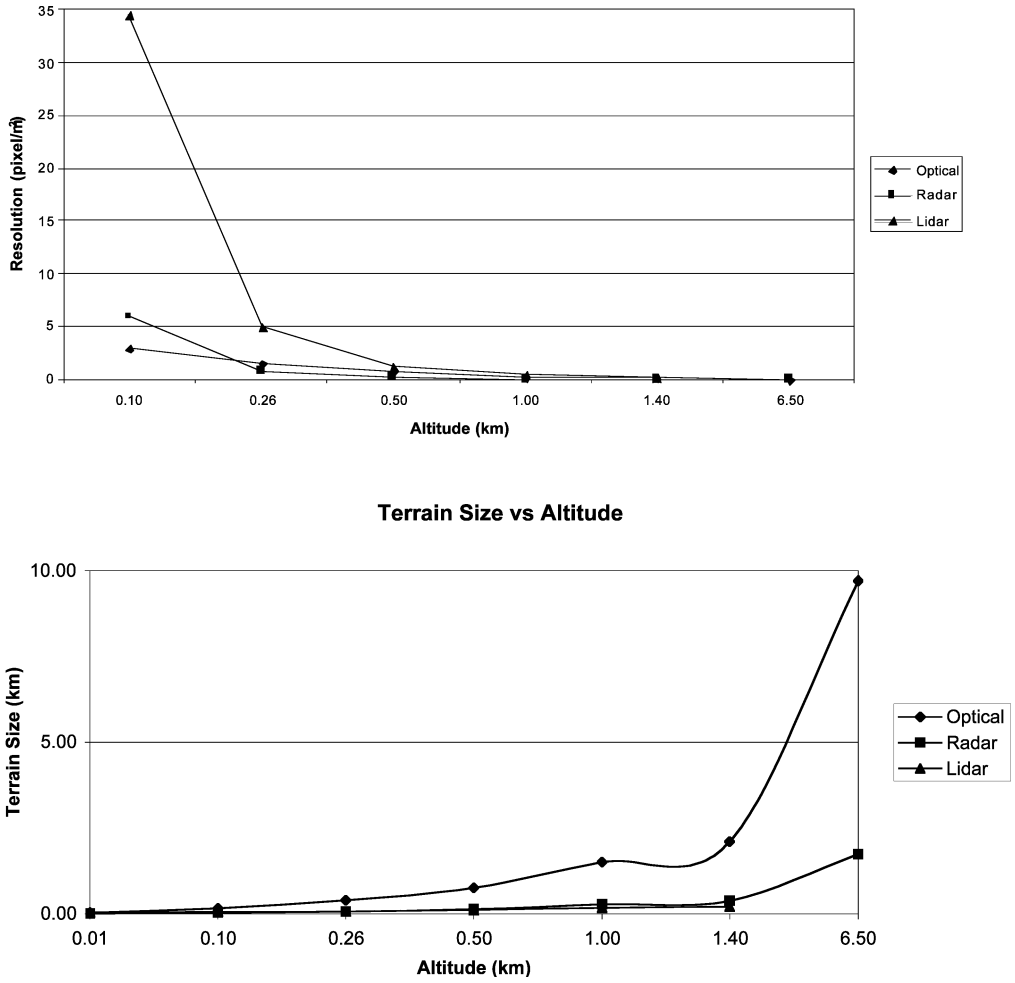

Fig. 8. Operating parameters for determining certainty rules.

lidar has better imaging resolution than the radar and camera, while the camera can image a larger area of the terrain. By extrapolating between these two constraints, we can construct certainty rules applicable to each sensor. Based on our analysis, the camera-based certainty rules are constructed as follows:

If distance is near, then β^{C} is high.
If distance is distant, then β^{C} is medium.
If distance is far, then β^{C} is low.

The lidar-based certainty rules are as follows:

If distance is near, then β^{L} is medium.
If distance is distant, then β^{L} is high.
If distance is far, then β^{L} is medium.

The radar-based certainty rules are as follows:

If distance is near, then β^{R} is low.
If distance is distant, then β^{R} is medium.
If distance is far, then β^{R} is high.

This information fusion framework allows data from additional sensors to be easily combined by allowing the construction of the certainty rules to reside on the sensor side.

TABLE II
Sensor Operating Parameters

Operating Parameter	Radar	Lidar	Camera
Minimum Range	100 m	0.5 m	0 m
Maximum Range	10 km	1.5 km	6.5 km
Resolution	4.4 m @ 1 km	.025 m @ 10 m	1.25 mrad/pixel
FOV	$\pm 10^{\circ} \times \pm 10^{\circ}$	$\pm 5^{\circ} \times \pm 5^{\circ}$	$\pm 73.4^{\circ} \times \pm 73.4^{\circ}$
Image Size	266×266 m @ 1 km 64×64 pixels	200×200 m @ 1.3 km 100×100 pixels	8 km×8 km @ 8 m/pixel 1024×1024 pixels
Detectable Features	Altimetry Slope Roughness	Slope Roughness	Surface features

In addition to constructing certainty rules, we must deal with the "unknown" map cells added during the transformation process discussed above. During the data transformation process, a number of cells embedded within the hazard map are given

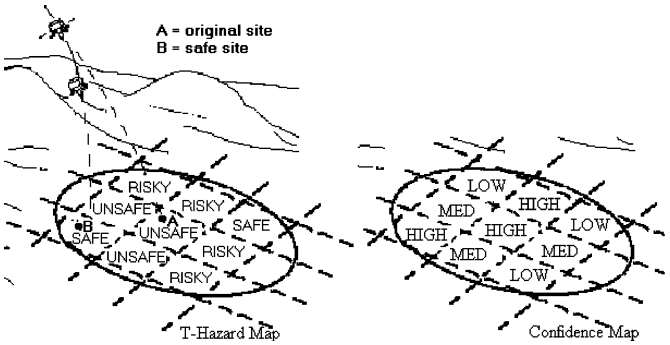

Fig. 9. Selecting a safe landing site for spacecraft touchdown.

the unknown value. This value designates a region of the terrain that an individual sensor is unable to view due to device constraints (field-of-view, resolution, size, etc.). To address this issue, we add certainty rules during the integration process as follows:

> If $h_{i,j}$ is unknown, then $\beta_{i,j}$ is zero
> else $\beta_{i,j}$ is unchanged

where i,j is the index of each cell in the T-hazard map, $h_{i,j}$ is the cell hazard map value, and $\beta_{i,j}$ represents the certainty factor associated with each cell. These rules, in effect, ensure that the system will not incorporate sensor data that has an unknown cell value into the integration equation.

An additional situation we address is when a high certainty factor is not provided by any of the sensors. For example, hazard map values from each sensor may have conflicting values, but also have an associated low confidence factor. For example, based on the following,

If β^{L} is low, then h^{L} is safe.
If β^{R} is low, then h^{R} is risky.
If β^{C} is low, then h^{C} is very-risky.

The combined values associated with safe, risky, and very-risky will result in a risky hazard value but with a low certainty factor. To ensure spacecraft safety, the certainty factor of the F-hazard map is calculated so that, during the actual site selection process, we prefer locations in which we have more confidence in the data. To address this preference, we produce a certainty map for the F-hazard map that can be used in the actual site selection process. We thus ensure that safe cells with a high certainty factor are preferred over safe cells with a low certainty value. To calculate the certainty factor of the resulting hazard map, we use the following equation:

$$B_{i,j} = \frac{\sum_{k=1}^{n} \beta_{i,j}^{k}}{n} \tag{7}$$

where $B_{i,j}$ represents the fused certainty factor associated with each cell and n is the number of on-board terrain sensors. In this case, unknown cells are given a certainty factor of zero since we prefer terrain regions in which all sensors provide concrete information.

Once calculated, the fused hazard and certainty maps are used to select a safe landing site. In our current application, the safe landing site is chosen as the safest site with the highest confidence factor located nearest to the original landing location (Fig. 9).

III. MULTI-SENSOR FUSION GRAPHICAL SIMULATOR

A graphical simulation testbed for displaying a spacecraft landing on a planetary terrain is used for evaluation and testing of the multi-sensor information fusion approach (Fig. 10). Fig. 10(a) depicts snapshots of the spacecraft landing simulation run on a typical Mars terrain while Fig. 10(b) shows the sensor visualization window which displays the sensor data input and corresponding hazard maps derived by the algorithm. The hazard map output calculated from the multi-sensor fusion algorithm is displayed at the bottom right-hand corner of Fig. 10(b). This visualization tool can incorporate a wide variety of digital elevation maps (DEMs) that represent different terrains and automatically update current spacecraft dynamic parameters during EDL operations. An additional feature is that data from multiple sensors can easily be incorporated and displayed to the user. The simulation testbed is used to validate and determine the performance of both individual and integrated sensors for hazard assessment and safe site selection. The testbed allows for technology validation under varied environmental conditions, including diverse terrain types, various altitudes, and different lighting conditions. Algorithm performance assessment includes factors such as computational speed, errors in assessment, and comparison with ground truth. For our application, the input parameters to the simulation are: spacecraft conditions (location/pose and velocity), terrain types (rock field, craters, cliff walls, flat surfaces), and terrain sensors (number of sensors, field-of-view, resolution, noise).

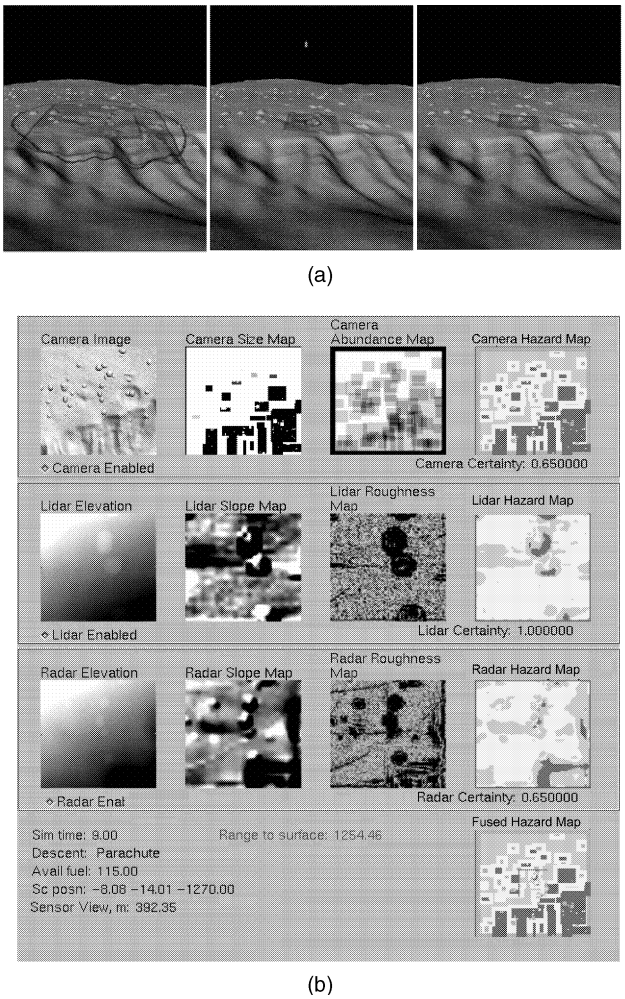

Fig. 10. Graphical simulation. (a) Spacecraft descent profile. (b) Sensor visualization window.

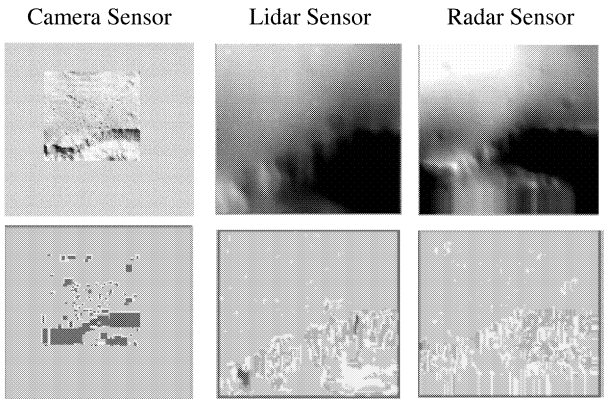

Fig. 11. Top row: sensor imagery data. Bottom row: derived hazard map.

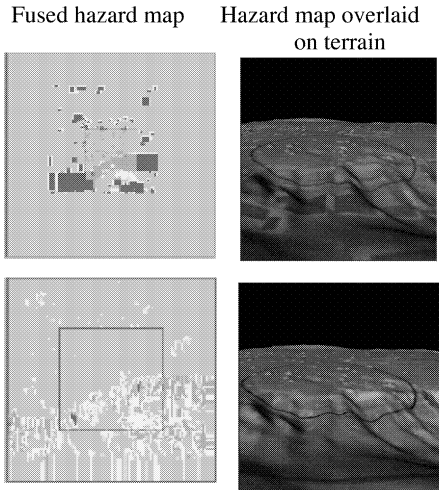

Fig. 12. Top row: F-hazard map with camera, lidar, and radar sensor. Bottom row: F-hazard map with lidar and radar sensor.

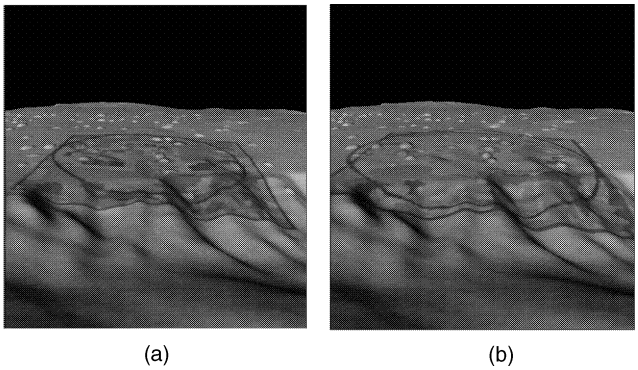

Fig. 13. Terrain snapshots comparing F-hazard maps derived from different sensor suites. (a) F-hazard map with camera, lidar, and radar sensors. (b) F-hazard map with lidar and radar sensors.

The output that is analyzed includes: selected site safety comparing different sensor suites and site safety as compared with ground truth.

Figs. 11–13 shows results comparing a simulation run with active camera, lidar, and radar sensors versus the same simulation run with only the lidar and radar sensors active. We ran approximately 50 simulation runs on the terrain segment, with different designated initial landing locations, spacecraft parameters, and sensor characteristics. In all cases, we compared the multi-sensor algorithm output based on different active sensor suites. We note that although the inclusion of the camera sensor increases the computational processing time of the algorithm, it enables identification of hazards that are not observable by the lidar and radar sensor alone. Based on our simulation runs, we have also verified that information from multiple sensors can effectively be combined to enable selection of safe landing sites during descent. The integration of data from multiple sensors allows the site selection algorithm to choose safe sites for landing by incorporating different terrain characteristics into the terrain assessment process. By using a diverse set of input data from redundant and complementary sensors, the system can reduce and correct errors that may be produced by a single sensor.

IV. LIMITATIONS

There are two main limitations associated with the multi-sensor information fusion methodology, namely: sensor pointing and certainty factors. During the landing simulation, we assume that the sensor pointing angle is downward-looking, toward the terrain surface. During descent, if the spacecraft is commanded to change orientation, the sensors will be reoriented relative to the direction of spacecraft movement. This characteristic is not directly incorporated into the simulation environment and thus could affect the results extracted from the data transformation process. The second limitation lies in the derivation of the certainty factors. In the simulation, the certainty map is constructed based on the distance of the spacecraft from the surface. Other factors that are derived from the actual sensor characteristics, such as the effect of sun angle on the performance of the camera sensor, should be incorporated into development of the certainty rules for each sensor. This will allow for a more precise derivation of the certainty factors associated with the sensor data output.

V. CONCLUSIONS

This paper presents a novel multi-sensor information fusion method for terrain classification from a safety standpoint. The fusion strategy directly incorporates information regarding the terrain characteristics extracted from heterogeneous active and passive sensors. The implementation of the fuzzy logic methodology for fusing sensed data is shown to provide a natural framework for representing the safety of the terrain for spacecraft landing. Through simulation, it is shown that the integration of fuzzy logic rules for terrain assessment allows the construction of an autonomous fusion strategy for safe spacecraft landing that deals with the real-world uncertainty inherent in natural environments. Future research will focus on incorporating additional sensors such as an infrared camera and additional constraints such as science value for selecting the final landing site.

ACKNOWLEDGMENTS

The development of the lidar sensor model and initial simulation package by Andrew Johnson of JPL is gratefully acknowledged. Thanks are due to Gene Chalfant, Max Bajracharya, and Paul Stuart of JPL for development of the graphical testbed used to test the multi-sensor information fusion methodology.

REFERENCES

[1] Golombek, M. P., Cook, R. A., Moore, H. J., and Parker, T. J. (1997)
Selection of the Mars Pathfinder landing site.
Journal of Geophysical Research, **102**, E2 (Feb. 1997), 3967–3988.

[2] Grant, J. (2003)
Overview of the landing site selection process and workshop goals.
Presented at the 4th Mars Exploration Rover Landing Site Selection Workshop, Pasadena, CA, 2003.

[3] Bernard, D. E., and Golombek, M. P. (2001)
Crater and rock hazard modeling for Mars landing.
In *Proceedings of AIAA Space Conference*, Albuquerque, NM, Aug. 2001.

[4] Johnson, A., Klumpp, A., Collier, J., and Wolf, A. (2001)
LIDAR-based hazard avoidance for safe landing on Mars.
Presented at the AAS/AIAA Space Flight Mechanics Meeting, Santa Barbara, CA, Feb. 2001.

[5] Johnson, A. E., and Skulsky, E. D. (2002)
Descent speed testing of a hazard detection system for safe landing on Mars.
In *Proceedings 25th AAS Guidance and Control Conference 2001*, Feb. 2002, AAS-02-024.

[6] Cheng, Y., Johnson, A., Matthies, L., and Wolf, A. (2001)
Passive imaging based hazard avoidance for spacecraft safe landing.
i-SAIRAS, Montreal, Canada, 2001.

[7] Bajracharya, M. (2002)
Single image based hazard detection for a planetary lander.
In *Proceedings of the World Automation Congress*, Orlando, FL, June 2002.

[8] Strandmoe, S. E.. Jean-Marius, T., and Trinh, S. (1999)
Toward a vision based autonomous planetary lander.
In *Proceedings of the AIAA GNC Conference*, Portland, OR, Aug. 1999.

[9] Waltz, E., and Llinas, J. (1990)
Multisensor Data Fusion.
Dedham, MA: Artech House, 1990.

[10] Zadeh, L. A. (1965)
Fuzzy sets.
Information and Control Journal, **12** (1965), 338–353.

[11] Howard, A., and Seraji, H. (2001)
Vision-based terrain characterization and traversability assessment.
Journal of Robotic Systems, **18**, 10 (2001), 577–587.

[12] Howard, A., and Seraji, H. (2001)
An intelligent terrain-based navigation system for planetary rovers.
IEEE Robotics and Automation Magazine, **8**, 4 (Dec. 2001).

[13] Tunstel, E., Lippincott, T., and Jamshidi, M. (1997)
Behavior hierarchy for autonomous mobile robots: Fuzzy-behavior modulation and evolution.
International Journal of Intelligent Automation & Soft Computing, **3**, 1 (1997), 37–50.

Ayanna Howard (M'91—SM'04) earned her B.S. in electrical engineering from Brown University, Providence, RI, and her M.S. and Ph.D. in electrical engineering from the University of Southern California, Los Angeles, in 1994 and 1999, respectively.

Since 1991, she has been at NASA's Jet Propulsion Laboratory, California Institute of Technology where she has led research efforts on various projects utilizing vision, fuzzy logic, and neural network methodologies. At JPL, she is a senior member of technical staff with the Mobility Systems Concept Development Section, and serves as the deputy manager of the Strategic University Research Partnership Office under the office of the chief scientist.

Dr. Howard has published over 50 written works on the successful use of artificial intelligence in a number of projects—from intelligent terrain assessment algorithms for landing on Mars to autonomous rover navigation for planetary surface exploration. She has released over 10 software and hardware technology innovations for licensing to the public, including the Artificial Intelligence (AI) Toolkit. To date, her unique accomplishments have been documented in over 12 featured articles—including being named as one of the world's top young innovators of 2003 by *Technology Review*, MIT's magazine of innovation and in TIME magazine's Innovator series "Rise of the Machines." Among her other achievements, she has received several NASA Space Act Awards for technical achievement and currently serves as Associate Editor for the *International Journal of Intelligent Automation and Soft Computing*.

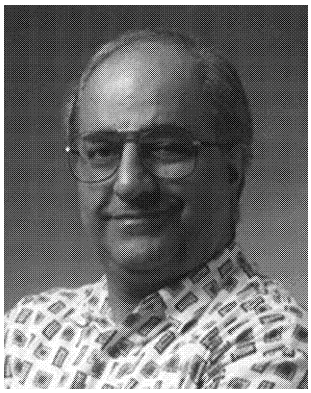

Homayoun Seraji (SM'87—F'98) graduated with a B.Sc. (First Class Honours) in electronics from the University of Sussex, England, in 1969, and earned his Ph.D. in multivariable control at the University of Cambridge, England, in 1972. He won a Cambridge Research Fellowship from St. John's College, and conducted post-doctoral research and teaching for two years.

In 1974, he joined Sharif (formerly Arya-Mehr) University of Technology, Iran, as a Professor of Electrical Engineering and was involved in teaching and research in modern control for ten years. He was selected as a U.N. Distinguished Scientist in 1984 and spent one year at the University of New Mexico, as a visiting professor. He joined Jet Propulsion Laboratory in 1985 as a senior member of technical staff and taught part-time at Caltech. Since 1991, he has been the group supervisor leading and managing a group of over 20 engineers and researchers in the Telerobotics Research and Applications Group. During his 17 year tenure at JPL, he has conducted extensive research that has led to major contributions in the field of robot control systems, particularly in: adaptive robot control, control of dexterous robots, contact control, real-time collision avoidance, and mobile robot navigation.

Dr. Seraji has received the NASA Exceptional Engineering Achievement Award in 1992 and seven NASA Major Space Act Awards in 1995, 1997, and 2000. The outcome of Dr. Seraji's research in controls and robotics has been published in over 90 journal papers, more than 100 conference publications, and 11 patents. In 1996, he was appointed a senior research scientist at JPL in recognition of his significant individual contributions in the fields of controls and robotics. Dr. Seraji was selected a fellow of IEEE in 1997 for his contributions to robotic control technology and its space applications.